JACS
JOURNAL OF THE AMERICAN CHEMICAL SOCIETY
Article
pubs.acs.org/JACS

From Seconds to Femtoseconds: Solar Hydrogen Production and Transient Absorption of Chalcogenorhodamine Dyes

Randy Pat Sabatini,[†,§] William T. Eckenhoff,[†,§] Alexandra Orchard,[‡] Kacie R. Liwosz,[‡] Michael R. Detty,[‡] David F. Watson,[‡] David W. McCamant,*[,†] and Richard Eisenberg*[,†]

[†]Department of Chemistry, University of Rochester, Rochester, New York 14627, United States
[‡]Department of Chemistry, University at Buffalo, The State University of New York, Buffalo, New York 14260, United States

Supporting Information

ABSTRACT: A series of chalcogenorhodamine dyes with oxygen, sulfur, and selenium atoms in the xanthylium core was synthesized and used as chromophores for solar hydrogen production with a platinized TiO_2 catalyst. Solutions containing the selenorhodamine dye generate more hydrogen [181 turnover numbers (TONs) with respect to chromophore] than its sulfur (30 TONs) and oxygen (20 TONs) counterparts. This differs from previous work incorporating these dyes into dye-sensitized solar cells (DSSCs), where the oxygen- and selenium-containing species perform similarly. Ultrafast transient absorption spectroscopy revealed an ultrafast electron transfer under conditions for dye-sensitized solar cells and a slower electron transfer under conditions for hydrogen production, making the chromophore's triplet yield an important parameter. The selenium-containing species is the only dye for which triplet state population is significant, which explains its superior activity in hydrogen evolution. The discrepancy in rates of electron transfer appears to be caused by the presence or absence of aggregation in the system, altering the coupling between the dye and TiO_2. This finding demonstrates the importance of understanding the differences between, as well as the effects of the conditions for DSSCs and solar hydrogen production.

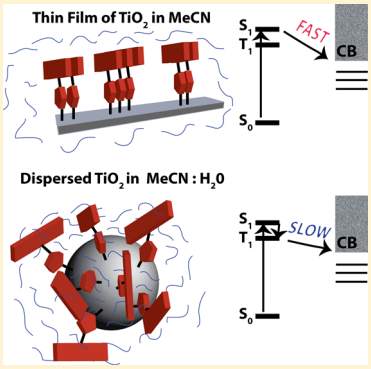

INTRODUCTION

In October 2011, the world's population passed the 7 billion mark with a projection of reaching 9 billion people by 2043.[1] Any growth in population is also accompanied by a growth in energy consumption, which, when combined with industrialization in developing countries, leads to an expected energy consumption growth of 56% between 2010 and 2040, from 524 $\times$ 10^{15} to 820 $\times$ 10^{15} Btu.[2] At present, 66% of the world's energy consumption is generated by the burning of fossil fuels.[3] Projections forward suggest a similar energy production profile with the attendant problem of increasing CO_2 emissions and consequent global climate change. It is therefore essential that scientific and technological efforts are able to make carbon-neutral energy more viable in the decades ahead. The most promising strategy for long-term, sustainable, carbon-neutral energy resides in using solar energy, as only a small fraction of the total sunlight hitting the Earth would need to be utilized.[4] One of the many challenges of solar energy is storing it, which can be done most efficiently in chemical bonds, as in photosynthesis. In artificial photosynthesis, the key energy-storing reaction is the splitting of water into its constituent elements, allowing the generated H_2 to be harvested and stored as a fuel.[5]

Efforts on this solar hydrogen production date back to 1972 and the seminal experiments by Fujishima and Honda[6] using titanium dioxide (TiO_2), Pt electrodes, and UV light. Much of the ensuing work has focused on either the reductive side or the oxidative side of solar water-splitting redox transformations. In 1977, Lehn and Sauvage succeeded in constructing a system for the reduction of protons to H_2 with a system that consisted of three components: $Ru(bpy)_3^{2+}$ as the light-absorber, a rhodium–bipyridine complex as an electron relay, and colloidal Pt as a catalyst.[7] In order to supply the electrons needed for proton reduction, triethanolamine was used as a sacrificial electron source. Similar reports by Kagan[8] and Grätzel[9] soon followed.

In the years since, progress has been made to improve upon these systems. Ruthenium complexes have been extensively researched as light harvesters,[10−19] but several characteristics make them less than ideal, including the high costs of the precious metal, low molar absorptivities (~15 000 M^{-1} cm^{-1}), excited state energies that do not align well with the solar spectrum, and photoinstability under prolonged irradiation. As an alternative to complexes of ruthenium and other noble metals (Ir, Pt) as light absorbers in these systems, organic dyes have been examined on a limited basis. Early studies employed the halogenated xanthene dyes Rose Bengal (ε_{559} = 90 400 M^{-1} cm^{-1})[20] and Eosin Y (ε_{525} = 112 000 M^{-1} cm^{-1})[20] in conjunction with either Pt/TiO_2 or methyl viologen/colloidal Pt for catalysis of H_2 formation.[21−24] More recently, Rose Bengal and Eosin Y were employed with a cobaloxime

Received: March 26, 2014
Published: May 6, 2014

   dx.doi.org/10.1021/ja503053s | J. Am. Chem. Soc. 2014, 136, 7740−7750

molecular catalyst to achieve 327 and 360 turnovers (TONs) of H_2, respectively.[25,26] These studies also indicated that the parent xanthene dye, fluorescein, did not function well, suggesting the possible need for a photosensitizer having heavy atoms and, therefore, a longer-lived $^3\pi\pi^*$ state.[21,26] However, the heavy-atom-containing dyes also exhibited very limited durability under irradiation conditions. One potential cause for dye decomposition was theorized to be facile cleavage of the C−X bond upon reductive quenching of the dye.

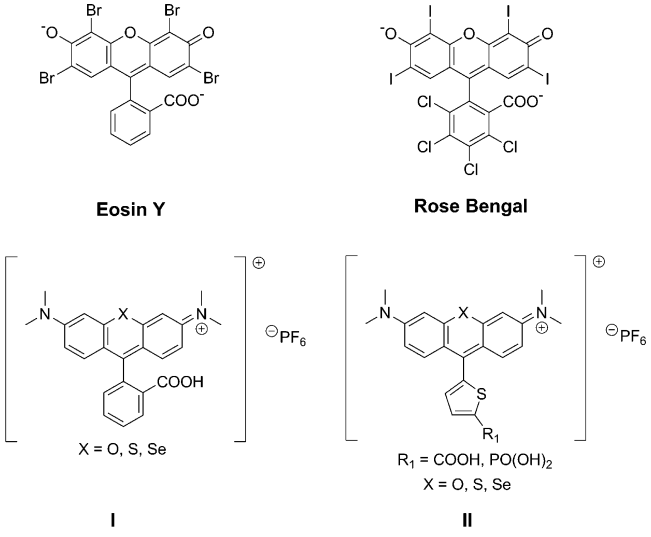

To overcome this pitfall, our efforts shifted to using rhodamine dyes, **I**, in which the central O atom was replaced by heavier group-16 elements, S and Se. Previous studies had shown that the generation of $^1O_2$ using these dyes increased in the order O < S < Se, consistent with increasing facility of intersystem crossing (ISC) of the initial excited state to the triplet manifold.[27] Use of **I** as the photosensitizer for H_2 formation was found to increase in the same order of activity, and with the addition of extra dimethylglyoxime ligand that was found to prolong catalyst activity, the **I-Se**/cobaloxime system achieved over 9000 TONs.[28] In the course of this work, **I-Se** was found to function through reductive quenching of its excited state and subsequent electron transfer from the reduced dye to the catalyst. However, if functioning catalyst was not present, the dye decomposed, indicating instability of the radical anion of **I-Se**.

On the basis of these and subsequent results,[29] oxidative quenching of the excited dye via electron transfer to the catalyst or an electron transfer mediator is preferable, since the oxidized dye is more stable than its $1e^-$ reduced form. While the dye may be directly connected to the catalyst to promote this pathway, success has been distinctly limited,[12,30−32] due in part to very fast back electron transfer.[32] Attaching the dye, instead, to a semiconductor can mitigate this problem. Dyes bound to TiO_2 have been shown to have ultrafast electron injection rates and much slower rates of recombination.[18,33−36] However, Johansson et al. have shown that, when a ruthenium complex is held far from the surface by extended ligands, electron transfer can occur in hundreds of nanoseconds.[37] After injection into the TiO_2 by the dye, the electron is transferred to an appropriate catalyst, and while the end goal is to use nonprecious metals or molecular catalysts attached to the semiconductor surface, Pt particles have worked well for model systems.[38−42]

Compared to the vast number of studies of dyes attached to TiO_2 for dye-sensitized solar cells (DSSCs) (see reviews and all references cited therein),[35,43−46] there is sparse literature on them in terms of applications for solar hydrogen generation. Some examples utilize square planar Pt(II) complexes,[47,48] ruthenium−bipyridyl complexes,[49,50] and organic chromophores[39,51] attached to the surface. Lakadamyali and Reisner, and Reynal et al. have recently established the picosecond to second time scales of electron transfer events in chromophore−TiO_2−catalyst systems for hydrogen production.[52,53] However, little research compares the differences in conditions between DSSCs and solar hydrogen-generating systems and investigates how these differences affect component activity in the systems. For example, Ru−bipyridyl complexes were found to exhibit different trends in relation to their linking group functionality when employed in DSSCs versus solar hydrogen-generating systems, presumably due to differences between the two environments.[50] A detailed study of what conditions affect activity and why would be useful in devising new systems.

Chalcogenorhodamine dyes, **II**, were used to address this issue. In previous studies by some of us,[54] carboxylic acid-functionalized **II** have been attached to TiO_2 and assessed for their ability to act as photosensitizers in DSSCs. On thin films, the dyes were found to form H-aggregates, which led to an increase in photocurrent and broadening of the range of absorption. Transient absorption spectroscopy on the nanosecond time scale showed that the selenium-containing dye injected an electron into TiO_2.[55] Replacement of the carboxylic acid with a phosphonic acid linker was shown to decrease the electron injection yield by a factor of 2,[56] but the stability of the system improved greatly. Whereas photocurrent measurements for the carboxylic acid-linked systems exhibited a decrease within 20−80 min as a result of dye desorption, the phosphonic acid dye systems remained stable on that time scale.[57] Additionally, only a marginal difference in the amount of photocurrent was observed by varying the chalcogen, presumably because ultrafast electron transfer precluded intersystem crossing into the triplet state.[57]

The present study examines chalcogenorhodamine dyes **II** for solar hydrogen production, focusing on the binding of the dyes to TiO_2 and the choice of chalcogen. Ultrafast transient absorption spectroscopy is used to probe the dyes in solution and on a variety of TiO_2 surfaces. Although previous DSSC results would suggest that there should be no difference in hydrogen production yields among the O-, S-, and Se-substituted species, we actually find that the choice of chalcogen is critical for successful hydrogen production. This indicates that slow electron injection occurs from the dye to TiO_2 in the aqueous conditions used for hydrogen production. Our results reconcile differences in the results of H_2 photogeneration described herein and previously reported photocurrent measurements using the same dyes on TiO_2 under DSSC-like conditions. The specific environmental causes of these differences are discussed.

EXPERIMENTAL SECTION

Equipment. All photolysis reactions were sealed and carried out in 40 mL reaction vials fitted with a pressure transducer. The vials were placed in a locally constructed 16-well photolysis apparatus in a water-cooled block at 15 °C, mounted on an orbital shaker. The cells were irradiated from below with high-power Philips LumiLEDs Luxeon ES Cool White (410−800 nm) 700 mA LEDs. The light power of each LED was set to 0.33 W and measured with an L30 A thermal sensor

dx.doi.org/10.1021/ja503053s | J. Am. Chem. Soc. 2014, 136, 7740−7750

and Nova II power meter (Ophir-Spiricon LLC). Each sample was degassed for 15 min with an 80:20 nitrogen:methane gas mixture. Over the course of the reaction, the pressure changes in the vials were recorded using a Labview program from a Freescale semiconductor sensor (MPXA4250AC6U). After photolysis, a sample of the headspace in each vial was analyzed by gas chromatography (Shimadzu GC-17A with a molecular sieve 5 Å column and TCD detector) to confirm the quantity of hydrogen gas produced versus the methane internal standard. Hydrogen evolution curves as shown in Figures 1

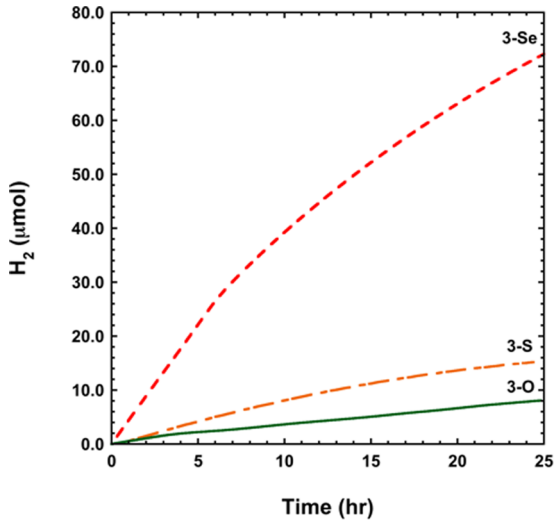

Figure 1. Hydrogen generation for phosphonic acid derivative dyes, showing much more activity for **3-Se** than for its oxygen and sulfur counterparts {5.1 mg of 3% Pt-TiO_2 (w/w), 1:1.2 MeCN:H_2O, [dye] = 80 μM, [ascorbic acid] = 0.1 M (pH 4.0), 5 mL}.

and 2 and S2, S4, S6, S8, S9, and S10 (Supporting Information) are the fits of the monitored sample pressure change. See Figure S1 (Supporting Information) for comparison between raw data and fits.

Transmission electron microscopy (TEM) and scanning TEM (STEM) were performed with an FEI Tecnai FEG STEM at 200 kV. Energy-dispersive X-ray spectroscopy (EDS) was performed with an EDAX spectrometer. Ground-state absorption spectra were taken with either a Shimadzu UV-1800 or a Cary 60 (Agilent) spectrophotometer. Diffuse reflectance spectroscopy was performed using a Dip Probe Coupler (Agilent) and a VideoBarrelino (Harrick).

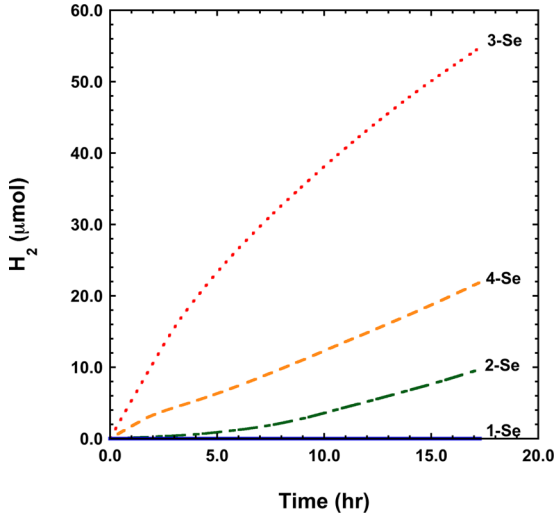

Figure 2. Comparison of hydrogen production of Se dyes **1-Se**–**4-Se** highlighting the effect of the anchoring functionality {5.1 mg of 3% Pt–TiO_2 (w/w), 1:1 MeCN:H_2O (1:1.2 MeCN:H_2O for **3-Se**), [dye] = 80 μM, [ascorbic acid] = 0.1 M (pH 4.0), 5 mL}.

For transient absorption (TA) spectroscopy, femtosecond laser pulses were produced by a regeneratively amplified titanium:sapphire laser (Spectra-Physics Spitfire) with a 1 kHz repetition rate. The actinic pump pulse at 550 nm was generated from a home-built noncollinear optical parametric amplifier. The probe was created by focusing an 800 nm beam through either a sapphire or calcium fluoride crystal, generating a white-light continuum. Color filters were used to select either the visible region of the spectrum (400–700 nm) or the near-infrared (NIR) region of the spectrum (825–1050 nm). The time delay was adjusted by optically delaying the pump pulse, with time steps increasing logarithmically.[58] Every other pump pulse was blocked by a chopper, and each probe pulse was measured by a CCD (Princeton Instruments, Pixis 100BR) after dispersion by a grating spectrograph (Acton, 300 mm fl, 150 gr/mm).

Liquid samples were held in a 2 mm cuvette. Samples probed in the visible region were kept at a maximum absorbance at the pump wavelength (550 nm) of around 0.5. Samples probed in the near-infrared region were made more concentrated (up to an absorbance of 1.0 at pump wavelength), to amplify the weak NIR signal. For work with dyes bound to TiO_2, thin films coated with transparent TiO_2 were immersed in a concentrated solution of the phosphonic acid derivatives. The slides were then washed with acetonitrile (MeCN) to remove loosely bound dye, and then placed in a 2 mm cuvette with acetonitrile. Scans were taken while continuously translating the sample, vertically for solution samples (1 mm/s) and both vertically (1 mm/s) and horizontally (2 mm/s) for dyes bound to TiO_2, in order to allow fresh sample to be probed. Pump powers at 550 nm were kept at ~70 nJ/pulse. On the basis of an estimated pump beam diameter of ~100 μm, ~10% of the TiO_2 attached dye molecules under irradiation were excited. This small number and the sample translation mitigate issues with potential long-lived charge separated states and the 1 kHz rep rate.

Kinetic traces were fit to the convolution of the Gaussian instrument response function (~800 fs) with a sum of exponential decays. The chirp of the probe was corrected by allowing time zero to vary depending on the wavelength. Stated errors in the fit parameters are $\pm 1\sigma$.

Materials. TiO_2 (Aeroxide P25), used in H_2-generating experiments, was purchased from Degussa. Potassium tetrachloroplatinate, 3-(diethylamino)propionic acid hydrochloride, and triethylamine were purchased from Sigma-Aldrich. Ascorbic acid was purchased from Fisher Scientific. Acetonitrile was purchased from Fisher Scientific and J.T. Baker. Methanol was purchased from Fisher Scientific and EMD Chemicals. Concentrated hydrochloric acid was purchased from EMD Chemicals. Triethanolamine was purchased from Alfa Aesar. Unless specified otherwise, all other organic reagents and solvents were purchased from Sigma-Aldrich. Tetrahydrofuran (THF) was distilled from sodium benzophenone ketyl prior to use. Other reagents and solvents were used without further purification.

Photolysis Reactions. In a typical experiment, 5.1 mg of Pt–TiO_2 was weighed out in a 40 mL vial followed by addition of 2.0 mL of a stock solution of rhodamine dye (2×10^{-4} M) in MeCN, which was diluted by addition of another 0.5 mL of MeCN. (For series **3**, the 2.0 mL of stock solution was 1.8 mL of CH_2CN and 0.2 mL of H_2O, to aid in solubility.) Each vial was then sonicated in the dark for 30 s. Finally, 2.5 mL of aqueous 0.2 M ascorbic acid solution (pH 4.0) was added, bringing the total volume to 5.0 mL. Reaction solutions were quickly transferred to the photolysis apparatus and degassed at 15 °C for 15 min. Any pH values listed correspond to the pH of the aqueous solution of the sacrificial donor before mixing with acetonitrile, also known as ${}^{w}_{w}$pH. A more accurate value for the pH of the mixed solvent, ${}^{s}_{s}$pH, can be found by using the equation $\delta = {}^{s}_{w}\mathrm{pH} - {}^{s}_{s}\mathrm{pH}$,[15,59] where ${}^{s}_{w}$pH is the measured pH value of the mixture. For solutions of 50% and 45% $MeCN_{(aq)}$, the ${}^{s}_{w}$pH values obtained after addition of dye solution to the pH 4 solution of ascorbic acid were 4.83 and 4.75, respectively, corresponding to ${}^{s}_{s}$pH values of 5.1 and 4.9, respectively.

dx.doi.org/10.1021/ja503053s | J. Am. Chem. Soc. 2014, 136, 7740–7750

RESULTS

The specific chalcogenorhodamine dyes **1**–**4** employed in the present study as photosensitizers for hydrogen production are shown in Scheme 1. Dyes **1-O**;[60] **1-S**, **1-Se**;[61] **2-O**, **2-S**, **2-Se**;[62]

Scheme 1. Chalcogenorhodamine Dyes Used as Visible Light Absorbers for Hydrogen Generation on Pt–TiO_2

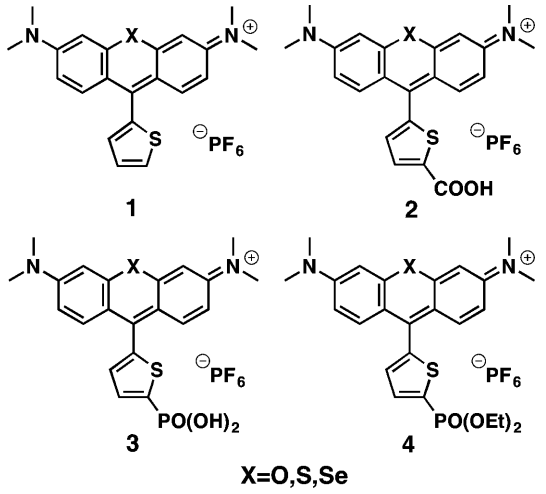

and **3-O**, **3-Se**, **4-O**, and **4-Se**[57] were synthesized according to literature procedures, whereas dyes **3-S** and **4-S** were prepared following the synthesis shown in Scheme S1 of the Supporting Information. Dyes **2**–**4** with X = O, S, Se are functionalized on the thiophene ring with a carboxylic acid, phosphonic acid, or phosphonate ester, respectively, for possible binding to TiO_2.

Unless otherwise specified, photolyses were conducted in 1:1 acetonitrile/water solvent mixtures at pH 4 with 0.1 M ascorbic acid as the sacrificial electron donor. For solubility, experiments with series **3** were performed in 1:1.2 acetonitrile/water solvent mixtures (see Experimental Section). Dye concentrations were 8×10^{-5} M. To the dye solutions was added 5.1 mg of 3% Pt–TiO_2 such that any binding between dye and TiO_2 occurred in situ. Reported TONs are described as the ratio of moles of hydrogen generated versus the moles of chromophore. Studies regarding the optimization of surface coverage and pH, as well as controls, can be found in the Supporting Information (Figures S2–S9).

The influence of the chalcogen in the dyes **3-O**, **3-S**, and **3-Se** was examined in a series of photolyses with 3% Pt–TiO_2 and 0.1 M ascorbic acid at pH 4. Irradiation and analyses were conducted as described in the Experimental Section. In 25 h, solutions containing **3-O**, **3-S**, and **3-Se** produced 20, ~30, and 181 TONs, respectively (Figure 1). Solutions containing **3-Se** were found to maintain hydrogen production for over 67 h, generating ~300 TONs (Figure S10).

A binding study was performed in order to ensure that the dyes were actually bound to TiO_2. Dyes **1-Se** and **4-Se** lack any viable binding group for attachment to TiO_2, while the carboxylic acid and phosphonic acid groups of **2-Se** and **3-Se**, respectively, are known to attach to TiO_2.[57,63,64] Under these conditions, solutions with **1-Se** were found to not generate any hydrogen, whereas solutions containing **2-Se** and **3-Se** produced H_2 upon irradiation, with **3-Se** significantly more active than **2-Se** (TONs of 137 and 25, respectively after 17 h). Solutions with **4-Se** produced 55 TONs (Figure 2), indicating that there is some in situ hydrolysis of the methyl ester (see the Supporting Information).

Figure 3 contains UV–vis absorption spectra of the ester dyes in acetonitrile and the acid dyes attached to both a TiO_2 thin film in acetonitrile and to colloidal TiO_2 in ethanol. When in solution, the dyes display a main absorption band as well as a Franck–Condon shoulder to higher energy. A smaller peak at ~375 nm is also present. The main absorbance peak shifts to lower energies as the chalcogen is changed from oxygen to sulfur and selenium, occurring at 574, 596, and 606 nm, respectively (Table 1). When the dyes are attached to a thin film of TiO_2 on glass, the strongest absorption occurs at a higher energy, and the spectrum is consistent with H-aggregation,[65,66] which has previously been shown for

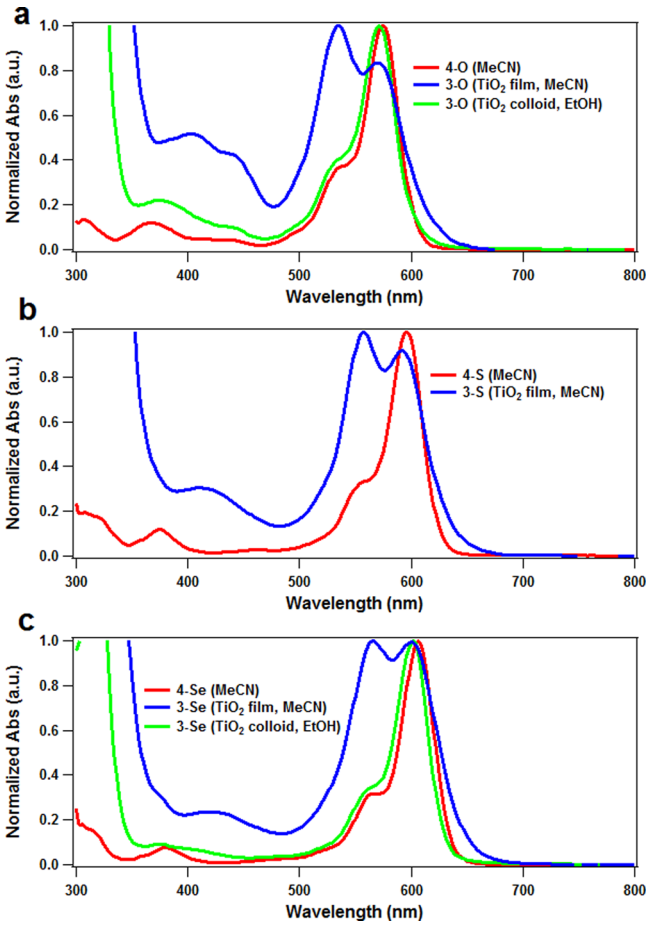

Figure 3. Absorption spectra of the phosphonate ester (**4**) and phosphonic acid (**3**) dyes in acetonitrile (red), bound to a TiO_2 film in acetonitrile (blue) and bound to colloidal TiO_2 particles in ethanol (green): (a) **4-O** and **3-O**, (b) **4-S** and **3-S**, and (c) **4-Se** and **3-Se**.

Table 1. Absorption Maxima Data for 4 Dyes in Acetonitrile Solution and 3 Dyes Attached to TiO_2 Thin Films in Acetonitrile and on Colloidal TiO_2 Particles in Ethanol

	λ_{max} (nm)		
chalcogen	**4-X** (MeCN)	**3-X**, on TiO_2 film (aggregate, monomer)	**3-X**, on TiO_2 colloid
O	574	534, 570	572
S	596	558, 592	–
Se	606	566, 600	602

dx.doi.org/10.1021/ja503053s | J. Am. Chem. Soc. 2014, 136, 7740–7750

chalcogenorhodamine dyes.[54] The ~375 nm peak shifts by about 40 nm to lower energy and gains intensity, possibly indicating a transition from the highest occupied molecular orbital (HOMO) of the dye directly to the conduction band of TiO_2.[67,68] As shown in Figure S11 (Supporting Information), the strong absorption at $\lambda < 350$ nm in the films is due to the TiO_2 absorption. Absorption data are presented in Table 1.

In contrast to the results on TiO_2 films, aggregation does *not* occur when the dyes are attached to TiO_2 in a colloidal suspension in ethanol, in which case the absorption spectra resemble those of the solution samples (Figure 3). However, it is more difficult to characterize the absorption spectrum of the dyes attached to the Degussa TiO_2 used for hydrogen production because of the large scattering background. Using a 0.1 mm cuvette to minimize scattering, the absorption spectra of **1-O** and **3-O** attached to Degussa TiO_2 were measured in 1:0.2 MeCN:H_2O and in 1:1.2 MeCN:H_2O including ascorbic acid at pH 4 [Figures 4 and S12 (Supporting Information)].

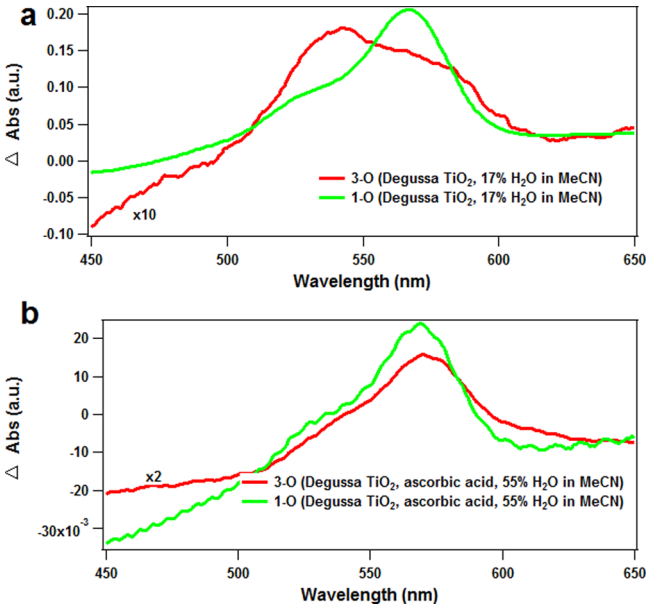

Figure 4. (a) Ground-state absorption of **3-O** and **1-O** attached to Degussa TiO_2 in 17% H_2O in MeCN. (b) Ground-state absorption of **3-O** and **1-O** attached to Degussa TiO_2 in 55% H_2O in MeCN with 0.1 M ascorbic acid at pH 4. Curves have been corrected for absorption of TiO_2 and ascorbic acid.

Dye **1-O** displays no aggregation in either solvent. Dye **3-O** displays H-aggregation when attached to TiO_2 in the 1:0.2 MeCN:H_2O solution. However, as seen in Figure 4, when the water concentration is increased, either in the absence or presence of ascorbic acid, no aggregation is observed.

Transient absorption (TA) spectroscopy was carried out on **4-O** in acetonitrile using both a visible and near-infrared probe. In Figure 5, the transient spectra (a,b) and kinetic traces (c,d) are shown. The ground-state absorption spectrum is also shown in Figure 5a as a dotted line, allowing comparison between it and the transient negative signal. Upon excitation by 550 nm light, the dye is excited into its first singlet excited state, resulting in a large positive signal at ~450 nm, due to excited state absorption (ESA). Between 525 and 700 nm, there is a negative signal, composed of both the ground-state bleach (GSB) and stimulated emission (SE). The stimulated emission appears to vanish in 14.8 ps, giving rise to a positive feature at ~640 nm and a bleach that mirrors the ground-state absorption spectrum with a minimum at ~570 nm. However, in the near-infrared region, a large negative feature begins to grow in with the same time constant. The growth of the near-infrared feature simultaneous with the loss of 600−670 nm SE signal is consistent with a dramatic shift of the SE to lower energy with a ~15 ps time constant. The molecule then returns to its ground state in 227 ps, as the 450 nm ESA, the 570 nm GSB, and the NIR SE decay back to baseline.

4-S was characterized in the same way, as shown in Figures 6a and S13 (Supporting Information). In the visible region, at early time delays, the transient spectra resemble that of **4-O**, with ESA at 450 nm and GSB and SE from 575 to 676 nm, indicating that the dye is in its first singlet excited state. However, in the NIR region, there is only a very small signal at $\lambda < 850$ nm and a small ESA from 950 to 1050 nm. A 0.35 ps lifetime is present, although its contributions are very small except at 640 nm. There is an analogous 15 ps time constant associated with a red-shifting of stimulated emission; however, this occurs on a much smaller scale in terms of both wavelength and amplitude. In **4-S**, the negative signal from 550−650 nm never matches the ground-state absorption, indicating that stimulated emission is still present in the longer wavelength region of this window. The excited state of the dye then relaxes back to the ground state in 71 ps, as both the ESA at ~450 nm and the negative signal (GSB and SE) decay back to baseline. No long-lived signal persists, implying that little to no triplet state is generated, in contrast to a previous study with a similar sulfur rhodamine dye, where the triplet yield was 0.23.[27]

Figures 6b and S14 (Supporting Information) show the TA results for **4-Se**. Again, we see the ESA at 450 nm, GSB and SE from 575 to 675 nm, a minor SE signal at 825 nm, and a small ESA from 900 to 1050 nm. Like **4-S**, **4-Se** has only trace amounts of shifting in its stimulated emission (0.87 ps). The ESA features at ~450 and 990 nm are consistent with initial population in its first singlet excited state. Over the first 50 ps, however, the SE signals are lost with a 27 ps time constant, visible in the kinetic traces at 675 and 825 nm. Within that same time frame, the ESA peak at 450 nm becomes a broad, featureless absorption band between 425 and 550 nm, and the peak at 990 nm increases, indicating a new excited state. The signal for both ESA peaks, as well as the GSB, remain for the duration of our experiment, a signature of a long-lived state, which we assign to the triplet state, T_1. In earlier work on **3-Se** in methanol, this state was found to decay with a ~0.6 μs lifetime.[56] The 27 ps time constant in our experiment is therefore attributed to intersystem crossing from S_1 to T_1, induced by spin−orbit coupling via the heavy atom effect of Se.

The energy level diagram in Figure 7 summarizes the excited state dynamics of the three dyes in solution.

TA spectra were also taken of the phosphonic acid-functionalized dyes attached to thin films of TiO_2, as shown in Figure 8 for the O, S, and Se derivatives. Upon excitation, the visible TA spectra look similar to the solution studies, with a few exceptions. In particular, the negative signal is broader, reflecting the bleach of the broader ground-state absorption. Within the broad negative signal, the relative magnitude of the monomer peak and the higher-energy aggregate peak are different than in the GS absorption spectrum. The largest amplitude occurs where the aggregate absorbs, suggesting that more of the aggregate is excited than the monomer. Only a very small amount of stimulated emission is present, which decays within a few picoseconds. The initial spectra in the near-

dx.doi.org/10.1021/ja503053s | J. Am. Chem. Soc. 2014, 136, 7740−7750

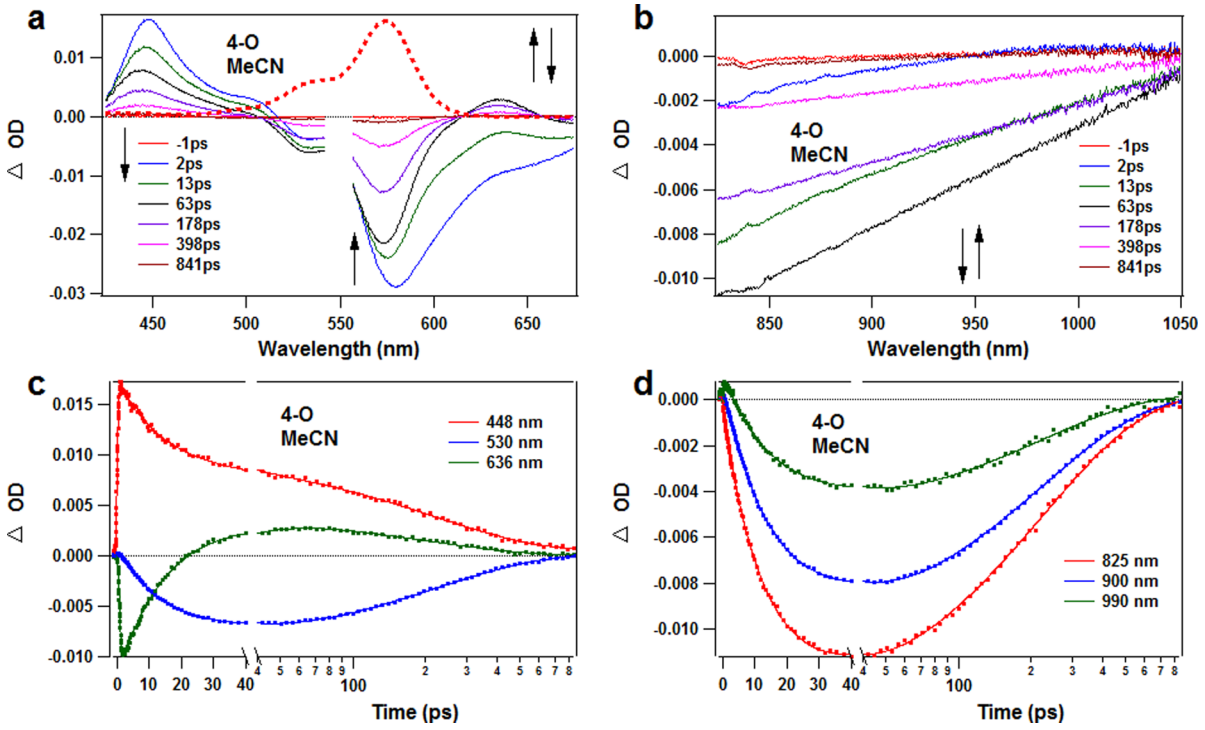

Figure 5. (a,b) Transient spectra of **4-O** in acetonitrile using a visible and near-infrared probe, respectively. (c,d) Kinetic traces of **4-O** in acetonitrile using a visible and near-infrared probe, respectively. Note that the ground-state absorption spectrum is the dashed curve in part a. Concentrations for NIR spectra are higher than concentrations for visible spectra to amplify the low signal.

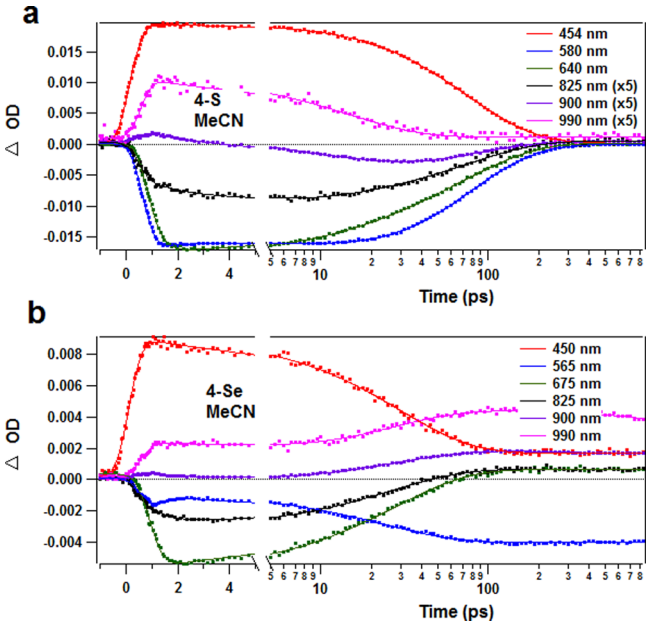

Figure 6. (a) Kinetic traces of **4-S** in acetonitrile using a visible and near-infrared probe, respectively. (b) Kinetic traces of **4-Se** in acetonitrile using a visible and near-infrared probe, respectively. Concentrations for NIR spectra are higher than concentrations for visible spectra to amplify the low signal.

infrared region, however, look very different from those of the solution studies. No appreciable amount of stimulated emission is apparent in this region at any time delay. Instead, only a positive signal is present for each dye–TiO_2 system.

Figure 9 shows the kinetic traces of the three dyes attached to a thin film of TiO_2 in MeCN. Although the dyes have very

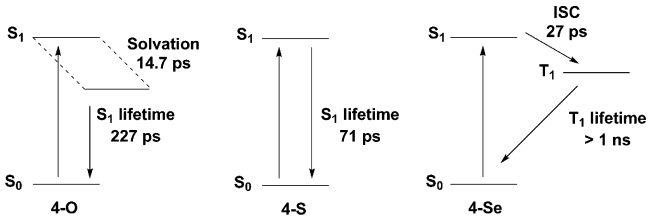

Figure 7. Energy level diagrams and dynamics of series **4** in solution.

distinctive dynamics in solution (see Figure 7), the kinetics of the adsorbed dyes look extraordinarily similar. Global fitting analysis was used to fit the kinetics at all the wavelengths simultaneously, using a common set of time constants with varying amplitudes at each wavelength. For each compound, three time constants were necessary to simultaneously fit all of the observed kinetics (Table 2). Each of the dyes, when attached to TiO_2, has three major time constants associated with its decay: 1.1–2.7, 25–39, and 160–240 ps. This differs greatly from the solution study work. **4-O** and **4-S** in solution experience solvent reorganization in ~15 ps and then undergo ground-state repopulation in 227 and 71 ps, respectively. **4-Se** in solution undergoes intersystem crossing in 27 ps, with the signal lasting the remainder of the experiment. When aggregated on a TiO_2 film, these compounds all behave fairly similarly, including time constants that cannot be explained by their solution-phase counterparts.

3-O and **3-Se** were also probed by TA using colloidal TiO_2 instead of a thin film. Figure 10 shows the visible and near-IR TA spectra of **3-O** attached to colloidal TiO_2 in ethanol. The spectrum looks very similar to that of the solution study, complete with red-shifting stimulated emission and a lack of aggregation. Kinetic fits of the data reveal two time constants: 17–35 and 170–270 ps. Figure S15 (Supporting Information)

dx.doi.org/10.1021/ja503053s | J. Am. Chem. Soc. 2014, 136, 7740–7750

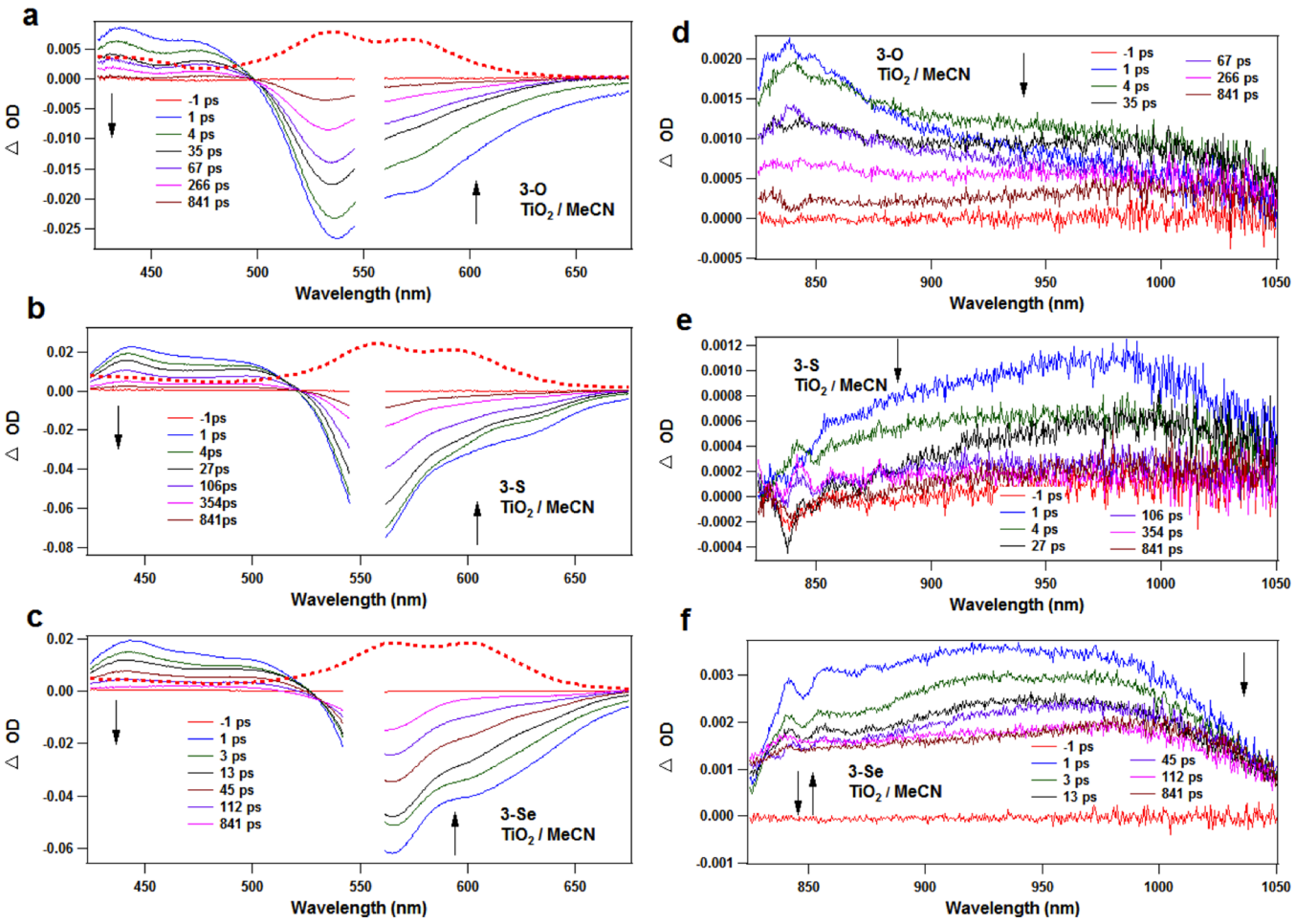

Figure 8. (a) Visible transient absorption spectra of **3-O** attached to a thin film of TiO_2 in acetonitrile; (b) visible, **3-S**; (c) visible, **3-Se**; (d) near-IR, **3-O**; (e) near-IR, **3-S**; (f) near-IR, **3-Se**. The ground-state absorption spectrum is shown as the dashed curve in (a,b,c).

shows the visible spectra and kinetic traces of **3-Se**, showing a 29 ps time constant, with the signal plateauing for the remainder of the experiment, just as in solution.

DISCUSSION

Hydrogen Evolution. Series **3** reveals that hydrogen production is heavily influenced by the chalcogen present in the xanthylium core, with solutions containing **3-O**, **3-S**, and **3-Se** generating 20, 30, and 181 TONs, respectively. The **3-Se** dye was found to have more overall hydrogen generated as well as a faster initial rate of hydrogen production, which correlates with its ability to populate the triplet state. Surprisingly, these results with a covalently *bound* dye on TiO_2 mirror previous results in which similar dyes were used *free* in solution with a cobaloxime catalyst.[28] In the prior study, the chromophore and catalyst were not attached and the quenching of the dye's excited state therefore occurred reductively, forming the anion of the dye, which in turn was able to transfer an electron to the catalyst. The quenching reaction was bimolecular and consequently benefitted from the long-lived $^3\pi\pi^*$ state of the dye. In the present study, however, the dyes are directly attached to the quencher, TiO_2, eliminating the need for slow bimolecular diffusion since electron injection from dyes bound to TiO_2 usually occurs in under a picosecond.[18,33,34] Such electron injection would occur directly from S_1, prior to any intersystem crossing, thus making the choice of chalcogen inconsequential. Our results instead show that the choice of chalcogen is very important and that *productive* electron transfer to TiO_2 under hydrogen-producing conditions must occur on a slower time scale.

Since the results of the hydrogen evolution experiments mirror those of the unattached chromophore−catalyst system,[28] care must be taken to determine that the dyes in this study are indeed bound to the TiO_2 during H_2 production. Our experiments probing the effect of the linking group (Figure 2) clearly indicate both that the **3** dyes are, in fact, bound to TiO_2 and that binding is necessary for hydrogen production (see the Supporting Information for further analysis).

Dynamics of Solution Study versus TiO_2 Thin Film. Besides some shifting in the stimulated emission region (see the Supporting Information for discussion), the dynamics of the dyes in solution are relatively straightforward. Dye **4-O** undergoes solvent reorganization in 14.7 ps and then returns to the ground state in 227 ps, whereas **4-S** undergoes a much less intense solvent reorganization in 15 ps and returns to the ground state in 71 ps. Dye **4-Se** undergoes intersystem crossing in 27 ps, and the triplet state remains for the duration of the experiment (>1 ns).

The dyes attached to thin films of TiO_2 show different kinetics than those in solution, with each dye exhibiting three time constants: 1−3, 25−40, and 160−240 ps. No substantial negative signal is present in the near-IR region of the spectra; instead, only a broad positive feature is present for each dye. Electrons in the conduction band of TiO_2,[18,69] as well as the

dx.doi.org/10.1021/ja503053s | J. Am. Chem. Soc. 2014, 136, 7740−7750

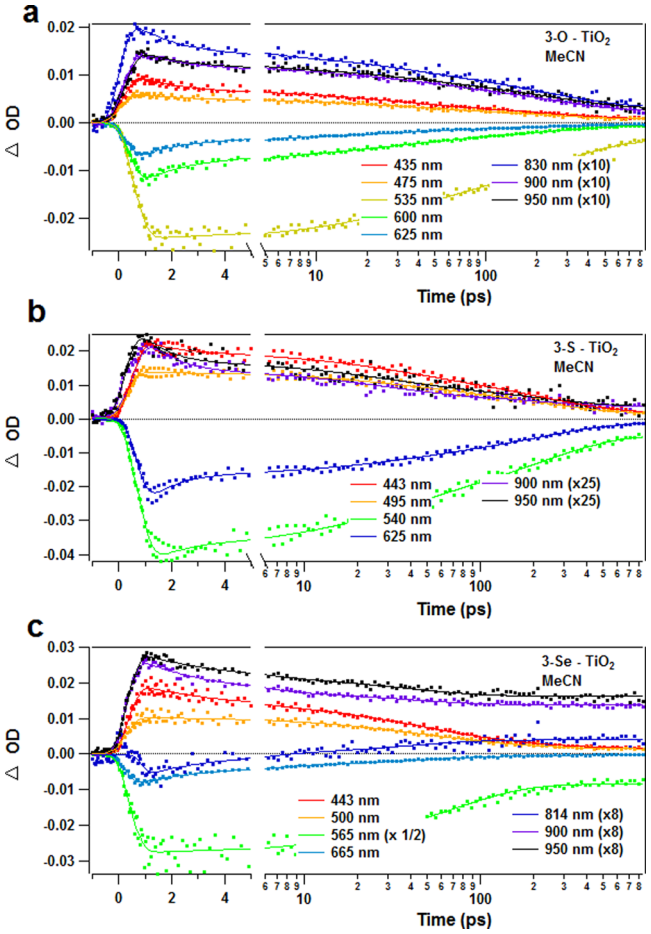

Figure 9. Kinetic traces for the phosphonic acid derivatized dyes attached to a thin film of TiO_2 in MeCN: (a) **3-O**, (b) **3-S**, and (c) **3-Se**. Global fitting was used to determine time constants.

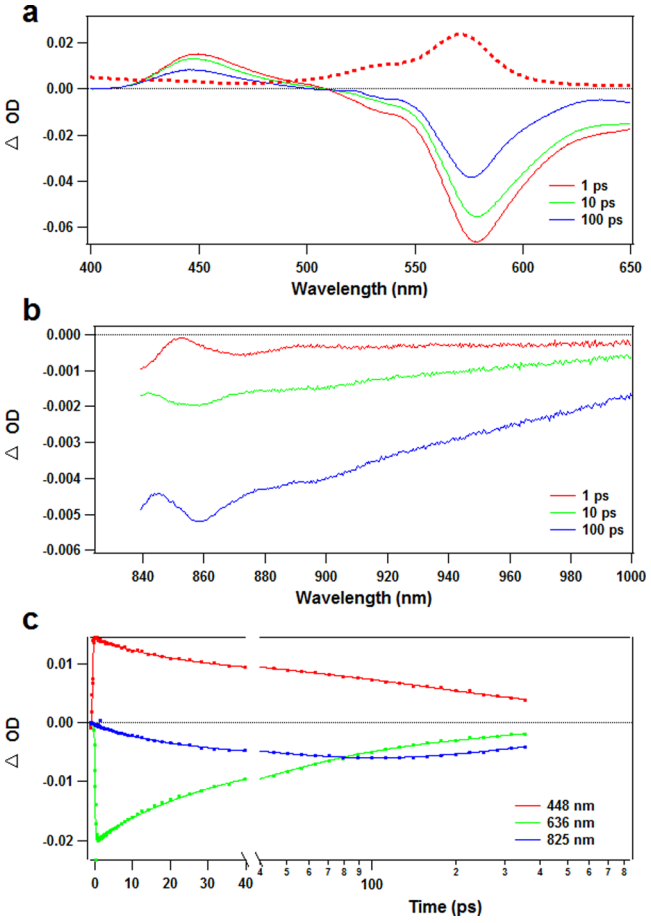

Figure 10. (a, b) Visible and near-IR transient spectra of **3-O** attached to colloidal TiO_2 in ethanol, respectively. (c) Kinetics of **3**-O attached to colloidal TiO_2 in ethanol. Both the visible and near-infrared regions look similar to the dye in acetonitrile. The ground-state absorption spectrum is shown as the dashed curve in part a.

trap states in ZrO_2,[67,70] have been shown to give rise to a broad absorption in the near-IR. Thus, these common time constants and features are consistent with ultrafast electron injection from the dye, directly from the S_1 into either the conduction band or surface traps states of TiO_2. Because the TA signal at 900 nm shows up instantaneously (see Figures 8 and 9), some percentage of the excited dye molecules has already injected an electron into TiO_2 within the instrument response time of our system (~800 fs). Only a very small signature of stimulated emission is present, which decays away with the fast time component, and the ground-state bleach associated with the aggregate species (blue edge) has no fast time component. This suggests that the fastest time component is either additional electron injection, as the process tends to be biphasic,[71,72] or the monomer species relaxing back to the ground state.

Since the medium and long time components appear to be similar between each dye, they are most likely associated with electron−hole recombination. Dyes **3-O** and **3-S** have little, if any, signal remaining after recombination occurs, implying complete ground-state repopulation. Dye **3-Se**, however, retains roughly 30% of the signal associated with the GSB. This is presumably the fraction of the photoexcited **3-Se** that did not inject into TiO_2, instead remaining in its triplet state after intersystem crossing. The 39 ps time constant of **3-Se** on the TiO_2 film may contain contributions of intersystem crossing of dyes that do not undergo fast electron transfer (eT) because of its similarity to the rate of intersystem crossing of **3-Se** in MeCN (27 ps). A similar fraction of **3-O** and **3-S** that does not inject into TiO_2 cannot be ruled out, although the lack of

Table 2. Major Time Constants for Series 3 in Acetonitrile and Series 4 Attached to a TiO_2 Film in Acetonitrile[a]

	solution kinetics[b]				thin film TiO_2 kinetics[c]		
4-X	τ_1 (ps)	τ_2 (ps)	τ_3 (ps)	**3-X**	τ_1 (ps)	τ_2 (ps)	τ_3 (ps)
O		14.8(0.3)	227(8)	O	1.74(0.16)	27(2)	240(16)
S	0.64(0.13)	15(2)	71(2)	S	1.1(0.2)	25(3)	220(17)
Se	0.87(0.16)	27(1)		**Se**	2.7(0.8)	39(9)	160(50)

[a]See Table S1 (Supporting Information) for fits of each individual wavelength. [b]Reported time constants for solution kinetics are the weighted averages of the different time constants measured for each wavelength. Numbers in parentheses are the standard deviations. [c]Reported time constants for TiO_2 kinetics are the result of global fitting analysis.

dx.doi.org/10.1021/ja503053s | J. Am. Chem. Soc. 2014, 136, 7740−7750

evidence in the kinetics suggests that, if it does exist, it is very small.

Colloidal TiO_2 and Hydrogen Production Using Degussa TiO_2. In the hydrogen evolution experiments, dispersed TiO_2 (Degussa P25) is utilized, as opposed to TiO_2 on thin films. Furthermore, the dyes do not show aggregation when bound to Degussa TiO_2 in a 55% water environment including ascorbic acid (Figure 4). Because the absorption spectrum of dye bound to Degussa TiO_2 in the 55% water environment resembles that of the dye bound to colloidal TiO_2 in ethanol, the colloidal TiO_2 is a better test-bed of what is occurring during photochemical generation of H_2. On colloidal TiO_2, the TA results resemble the solution study and indicate that eT to TiO_2 does not take place in <1 ns, differing from the experiments on thin films. However, eT must be occurring, in order to generate hydrogen. Reductive quenching by the sacrificial donor is ruled out as a possibility, as **1-Se** produces no hydrogen. The only other possibility is slow eT, which would elevate the importance of the triplet state. On the basis of the solution transient absorption work, only the selenium species generates any appreciable triplet state and is therefore the best dye for hydrogen production.

Previous Photocurrent Experiments versus Hydrogen Production. In the previous photocurrent work, both **3-O** and **3-Se** performed similarly when bound to a TiO_2 film in a MeCN environment, with **3-O** performing slightly better than **3-Se**. In that study the dyes were found to achieve IPCE values of 70−85%, implying a very efficient photochemical process of transferring electrons into the conduction band of TiO_2.[57] In our hydrogen generation experiments, **3-Se** greatly outperforms **3-S**, which performs similarly to **3-O**. The previous discussion of electron transfer rates helps to reconcile these differences. The photocurrent experiments are performed on thin films of TiO_2 in MeCN, where the dyes form aggregates and ultrafast electron injection occurs from the singlet excited state. The triplet state plays no role in the process, and each dye functions similarly. In hydrogen-evolution experiments, TiO_2 is in dispersed nanoparticulate form surrounded by both MeCN *and* H_2O, which prevents dye aggregation and produces a much slower rate of electron injection from the dyes. The triplet state then becomes important, with the dye containing selenium performing the best (Figure 11).

The difference in rates of electron transfer may be an effect of the presence or absence of dye aggregation on the surface of TiO_2, which occurs in conditions resembling the photocurrent work, but does *not* occur in conditions resembling hydrogen evolution. On TiO_2 thin films with a MeCN solvent, the dyes form H-aggregates, in which they are π-stacked upon one another. We have shown here that these dyes also aggregate on Degussa TiO_2 in a MeCN environment, but that the addition of water and ascorbic acid, as is necessary for hydrogen production, breaks up the aggregation (see Figure 4). Previous work on the carboxylic acid analogues has suggested that aggregation induces coplanarity between the thienyl group and the attached xanthene ring.[54] Any coplanarity between the two rings would increase the coupling between the two moieties and the semiconductor, thereby increasing the rate of electron injection when the dye is attached and aggregated on thin films of TiO_2, as in the photocurrent work. This extra coupling is absent when the dye is attached to either colloidal TiO_2 in ethanol or Degussa TiO_2 in the presence of ascorbic acid and a 55% aqueous solvent, as in hydrogen evolution experiments, resulting in slow electron transfer.

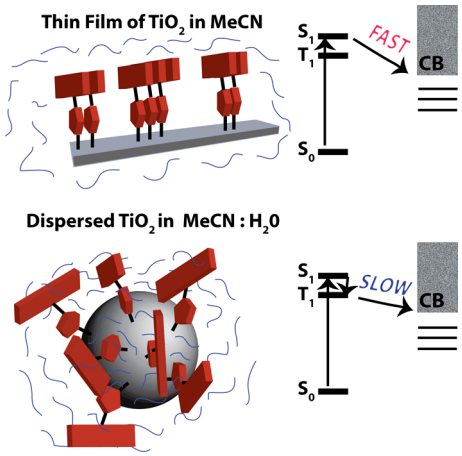

Figure 11. Schematic of differing rates of electron injection from dye into TiO_2. The pathway proceeds through the triplet state only when the dye is attached to the colloidal particles in the presence of water, upon which the dyes do not aggregate.

Previous Nanosecond Transient Absorption versus Ultrafast Transient Absorption. Previous transient absorption experiments on the nanosecond time scale were performed on **3-Se** attached to TiO_2 in the presence and absence of Li^+.[56] At 10 μs, a positive peak at 520 nm, attributed to the dye radical cation (due to electron injection into the conduction band of TiO_2), was observed only in the presence of Li^+ and was confirmed by comparing to the absorption spectrum of bound 3-$Se^{(+)}$ generated by chemical oxidation. Li^+ has been shown to increase the electron injection quantum yield by shifting the conduction band to more positive electrochemical potentials.[73] Attachment of **3-Se** to ZrO_2 yielded no peak at 520 nm with or without Li^+ at 10 μs,[56] as the conduction band for ZrO_2 is ∼1 eV higher in energy than that of TiO_2.

In order to compare with these slower spectroscopic experiments,[55,56] transient spectra were also obtained of **3-Se** on TiO_2 with 0.3 M Li^+, as well as **3-Se** on ZrO_2. The comparison between these data and **3-Se** on TiO_2 without added Li^+ is shown in Figure S16 (Supporting Information). Unlike the previous work, our experiments show no significant difference in the spectra or kinetics of **3-Se** on TiO_2, TiO_2 with Li^+, or ZrO_2 (Figure S16, Supporting Information). The lack of any dependence on the energy of the semiconductor's conduction band suggests that the observed ultrafast electron transfer is to the surface trap states. This is consistent with the fast recombination times measured in the kinetics of each dye on TiO_2 (Figure 9). Injection into trap states generally occurs when dyes are coupled strongly to the semiconductor.[70] For these dyes, the strong coupling can be attributed to aggregation-induced coplanarity of the rings (vide supra). Our observation of fast eT to trap states and subsequent recombination on the ∼200 ps time scale is at odds with the success of these dyes when used as sensitizers in previous DSSC experiments, which require a long-lived electron in the TiO_2 conduction band to allow for its migration to the electrode.[57] However, the DSSCs contained a combination of Li^+, 4-*tert*-butylpyridine, and acid, which are known to manipulate the conduction band and enhance the efficiency of the device, presumably by preventing eT to unproductive trap states. Hence, we attribute the success of these dyes in DSSCs, despite our observation of rapid eT and recombination,

dx.doi.org/10.1021/ja503053s | J. Am. Chem. Soc. 2014, 136, 7740−7750

to the unique solvent and ionic environment in which the DSSCs operate.

While electron injection appears to be occurring in our experiments, there is no 520 nm band, attributed to the radical cation of the dye, apparent in our spectra. However, in the previous work using TiO_2 with Li^+, the radical cation absorption peak at 520 nm sometimes had a rise time associated with it (the intermittence due to slight differences from slide to slide), indicating a process occurring within several hundred nanoseconds, similar to the time resolution of the system.[56] This nanosecond growth of the cation absorption band is likely due to an additional electron transfer from the triplet state, via the fraction of dye that does not inject on the ultrafast time scale. In our experiments at times less than 1 ns, the 520 nm peak is not observed because it is offset by the additional bleach associated with the fraction of dye that has not injected. We expect that the residual triplet state seen in Figure 9c performs electron injection on the hundreds of nanoseconds time scale, as has been seen in the nanosecond transient absorption work.

CONCLUSION

A series of chalcogenorhodamine dyes have been examined for the photochemical generation of hydrogen from aqueous protons. Attachment of the dye to TiO_2 is crucial for hydrogen generation, as no hydrogen was generated when a dye lacking a linking group was used. In contrast with previous photocurrent measurements, in which each TiO_2-attached dye performed roughly the same, the dyes show markedly different H_2 production based on the chalcogen present in the xanthene ring. The improved activity of **3-Se** is ascribed to the dye's ability to undergo intersystem crossing into the triplet state. When the dyes are attached to colloidal TiO_2, no ultrafast electron transfer is observed within 1 ns of photoexcitation, making a long-lived excited state vital for efficient hydrogen generation. Only the selenium-containing species forms an appreciable amount of the triplet state, which correlates well with its greater ability to generate H_2 upon irradiation.

Transient absorption spectra of the chalcogenorhodamine series attached to thin films of TiO_2 in neat acetonitrile, however, show indications of ultrafast electron transfer directly from the singlet state and subsequent recombination on the ~200 ps time scale. The discrepancy between the photocurrent and solar hydrogen production experiments is ascribed to a change in the coupling of the dyes to TiO_2, caused by aggregation-induced coplanarity between the thienyl group and the attached xanthene ring. Although the type of TiO_2 differs in each experiment, the solvent environment surrounding the TiO_2 plays the major role in determining the aggregation of the dye. Specifically, the aqueous environment of the H_2 experiments disrupts the aggregation of the dye molecules on the TiO_2 surface, slowing the rate of electron transfer by over 3 orders of magnitude. DSSCs and solar hydrogen-generating systems can differ dramatically in their solvent and TiO_2 morphology. The dramatic influence of the solvent on these heterogeneous electron transfer systems reminds us to use caution when applying lessons learned from DSSC work to related hydrogen production systems.

ASSOCIATED CONTENT

Supporting Information

Synthetic procedures, additional hydrogen evolution data, ground-state absorption spectra, transient spectra, tabulated time constants, and further discussion. This material is available free of charge via the Internet at http://pubs.acs.org.

AUTHOR INFORMATION

Corresponding Authors

mccamant@chem.rochester.edu
eisenberg@chem.rochester.edu

Author Contributions

[§]These authors contributed equally to this work.

Notes

The authors declare no competing financial interest.

ACKNOWLEDGMENTS

This work was supported by National Science Foundation Collaborative Research grants (CHE-1151789 to R.E. and D.M.W. and CHE-1151379 to M.R.D. and D.F.W). Additionally, D.W.M.. was supported as an Alfred P. Sloan Research Fellow ,and R.P.S. was supported by a National Science Foundation Graduate Research Fellowship. W.T.E. also wishes to thank the National Science Foundation for the American Competitiveness in Chemistry Postdoctoral Fellowship (CHE-1137057).

REFERENCES

(1) Seven Billion and Growing: The Role of Population Policy in Achieving Sustainability. http://www.un.org/esa/population/publications/technicalpapers/TP2011-3_SevenBillionandGrowing.pdf (accessed 12/03/2013).

(2) International Energy Outlook 2013. http://www.eia.gov/pressroom/presentations/sieminski_07252013.pdf (accessed 12/03/2013).

(3) Key World Energy Statistics 2012. http://www.iea.org/publications/freepublications/publication/kwes.pdf (accessed 12/03/2013).

(4) Lewis, N. S.; Nocera, D. G. *Proc. Natl. Acad. Sci. U. S. A.* **2006**, *103*, 15729.

(5) Concepcion, J. J.; House, R. L.; Papanikolas, J. M.; Meyer, T. J. *Proc. Natl. Acad. Sci. U. S. A.* **2012**, *109*, 15560.

(6) Fujishima, A.; Honda, K. *Nature* **1972**, *238*, 37.

(7) Lehn, J. M.; Sauvage, J. P. *Nouv. J. Chim.* **1977**, *1*, 449.

(8) Moradpour, A. A. E.; Keller, P.; Kagan, H. B. *Nouv. J. Chim.* **1978**, *2*, 547−549.

(9) Kalyanasundaram, K.; Kiwi, J.; Grätzel, M. *Helv. Chim. Acta* **1978**, *61*, 2720.

(10) Chen, C.-Y.; Wu, S.-J.; Wu, C.-G.; Chen, J.-G.; Ho, K.-C. *Angew. Chem., Int. Ed.* **2006**, *45*, 5822.

(11) Lundqvist, M. J.; Nilsing, M.; Lunell, S.; Akermark, B.; Persson, P. *J. Phys. Chem. B* **2006**, *110*, 20513.

(12) Li, C.; Wang, M.; Pan, J.; Zhang, P.; Zhang, R.; Sun, L. *J. Organomet. Chem.* **2009**, *694*, 2814.

(13) Hall, J. D.; McLean, T. M.; Smalley, S. J.; Waterland, M. R.; Telfer, S. G. *Dalton Trans.* **2010**, *39*, 437.

(14) Fukuzumi, S.; Kobayashi, T.; Suenobu, T. *Angew. Chem., Int. Ed.* **2011**, *50*, 728.

(15) McNamara, W. R.; Han, Z.; Yin, C. J.; Brennessel, W. W.; Holland, P. L.; Eisenberg, R. *Proc. Natl. Acad. Sci. U. S. A.* **2012**, *109*, 15594.

(16) Veikko, U.; Zhang, X.; Peng, T.; Cai, P.; Cheng, G. *Spectrochim. Acta Part A* **2013**, *105*, 539.

(17) Furlong, D. N.; Wells, D.; Sasse, W. H. F. *J. Phys. Chem.* **1986**, *90*, 1107.

(18) Tachibana, Y.; Moser, J. E.; Gratzel, M.; Klug, D. R.; Durrant, J. R. *J. Phys. Chem.* **1996**, *100*, 20056.

(19) Nazeeruddin, M. K.; Pechy, P.; Renouard, T.; Zakeeruddin, S. M.; Humphry-Baker, R.; Comte, P.; Liska, P.; Cevey, L.; Costa, E.;

Shklover, V.; Spiccia, L.; Deacon, G. B.; Bignozzi, C. A.; Gratzel, M. *J. Am. Chem. Soc.* **2001**, *123*, 1613.
(20) Seybold, P. G.; Gouterman, M.; Callis, J. *Photochem. Photobiol.* **1969**, *9*, 229.
(21) Shimidzu, T.; Iyoda, T.; Koide, Y. *J. Am. Chem. Soc.* **1985**, *107*, 35.
(22) Mau, A. W.-H.; Johanssen, O.; Sasse, W. H. F. *Photochem. Photobiol.* **1985**, *41*, 503.
(23) Hashimoto, K.; Kawai, T.; Sakata, T. *Nouv. J. Chim.* **1984**, *8*, 693.
(24) Misawa, H.; Sakuragi, H.; Usui, Y.; Tokumaru, K. *Chem. Lett.* **1983**, *12*, 1021.
(25) Zhang, P.; Wang, M.; Dong, J.; Li, X.; Wang, F.; Wu, L.; Sun, L. *J. Phys. Chem. C* **2010**, *114*, 15868.
(26) Lazarides, T.; McCormick, T.; Du, P.; Luo, G.; Lindley, B.; Eisenberg, R. *J. Am. Chem. Soc.* **2009**, *131*, 9192.
(27) Ohulchanskyy, T. Y.; Donnelly, D. J.; Detty, M. R.; Prasad, P. N. *J. Phys. Chem. B* **2004**, *108*, 8668.
(28) McCormick, T. M.; Calitree, B. D.; Orchard, A.; Kraut, N. D.; Bright, F. V.; Detty, M. R.; Eisenberg, R. *J. Am. Chem. Soc.* **2010**, *132*, 15480.
(29) Han, Z.; McNamara, W. R.; Eum, M.-S.; Holland, P. L.; Eisenberg, R. *Angew. Chem., Int. Ed.* **2012**, *51*, 1667.
(30) McCormick, T. M.; Han, Z.; Weinberg, D. J.; Brennessel, W. W.; Holland, P. L.; Eisenberg, R. *Inorg. Chem.* **2011**, *50*, 10660.
(31) Zhang, P.; Wang, M.; Li, C.; Li, X.; Dong, J.; Sun, L. *Chem. Commun.* **2010**, *46*, 8806.
(32) Peuntinger, K.; Lazarides, T.; Dafnomili, D.; Charalambidis, G.; Landrou, G.; Kahnt, A.; Sabatini, R. P.; McCamant, D. W.; Gryko, D. T.; Coutsolelos, A. G.; Guldi, D. M. *J. Phys. Chem. C* **2012**, *117*, 1647.
(33) Cherepy, N. J.; Smestad, G. P.; Gratzel, M.; Zhang, J. Z. *J. Phys. Chem. B* **1997**, *101*, 9342.
(34) Hannappel, T.; Burfeindt, B.; Storck, W.; Willig, F. *J. Phys. Chem. B* **1997**, *101*, 6799.
(35) Ardo, S.; Meyer, G. J. *Chem. Soc. Rev.* **2009**, *38*, 115.
(36) Stockwell, D.; Yang, Y.; Huang, J.; Anfuso, C.; Huang, Z.; Lian, T. *J. Phys. Chem. C* **2010**, *114*, 6560.
(37) Johansson, P. G.; Zhang, Y.; Abrahamsson, M.; Meyer, G. J.; Galoppini, E. *Chem. Commun.* **2011**, *47*, 6410.
(38) Patsoura, A.; Kondarides, D. I.; Verykios, X. E. *Appl. Catal., B* **2006**, *64*, 171.
(39) Abe, R.; Hara, K.; Sayama, K.; Domen, K.; Arakawa, H. *J. Photochem. Photobiol., A* **2000**, *137*, 63.
(40) Hirano, K.; Suzuki, E.; Ishikawa, A.; Moroi, T.; Shiroishi, H.; Kaneko, M. *J. Photochem. Photobiol., A* **2000**, *136*, 157.
(41) Abe, R.; Sayama, K.; Arakawa, H. *J. Photochem. Photobiol., A* **2004**, *166*, 115.
(42) Sabatini, R. P.; McCormick, T. M.; Lazarides, T.; Wilson, K. C.; Eisenberg, R.; McCamant, D. W. *J. Phys. Chem. Lett.* **2011**, *2*, 223.
(43) Grätzel, M. *J. Photochem. Photobiol. C* **2003**, *4*, 145.
(44) Grätzel, M. *Inorg. Chem.* **2005**, *44*, 6841.
(45) Hagfeldt, A.; Boschloo, G.; Sun, L.; Kloo, L.; Pettersson, H. *Chem. Rev.* **2010**, *110*, 6595.
(46) Anderson, N. A.; Lian, T. *Annu. Rev. Phys. Chem.* **2005**, *56*, 491.
(47) Jarosz, P.; Du, P.; Schneider, J.; Lee, S. H.; McCamant, D.; Eisenberg, R. *Inorg. Chem.* **2009**, *48*, 9653.
(48) Zhang, J.; Du, P.; Schneider, J.; Jarosz, P.; Eisenberg, R. *J. Am. Chem. Soc.* **2007**, *129*, 7726.
(49) Zheng, H.-Q.; Yong, H.; Ou-Yang, T.; Fan, Y.-T.; Hou, H.-W. *Int. J. Hydrogen Energy* **2013**, *38*, 12938.
(50) Bae, E.; Choi, W. *J. Phys. Chem. B* **2006**, *110*, 14792.
(51) Jin, Z.; Zhang, X.; Lu, G.; Li, S. *J. Mol. Catal. A: Chem.* **2006**, *259*, 275.
(52) Lakadamyali, F.; Reisner, E. *Chem. Commun.* **2011**, *47*, 1695.
(53) Reynal, A.; Lakadamyali, F.; Gross, M. A.; Reisner, E.; Durrant, J. R. *Energy Environ. Sci.* **2013**, *6*, 3291.
(54) Mann, J. R.; Gannon, M. K.; Fitzgibbons, T. C.; Detty, M. R.; Watson, D. F. *J. Phys. Chem. C* **2008**, *112*, 13057.
(55) Mulhern, K. R.; Detty, M. R.; Watson, D. F. *J. Phys. Chem. C* **2011**, *115*, 6010.
(56) Mulhern, K. R.; Detty, M. R.; Watson, D. F. *J. Photochem. Photobiol., A* **2013**, *264*, 18.
(57) Mulhern, K. R.; Orchard, A.; Watson, D. F.; Detty, M. R. *Langmuir* **2012**, *28*, 7071.
(58) Megerle, U.; Pugliesi, I.; Schriever, C.; Sailer, C. F.; Riedle, E. *Appl. Phys. B: Laser Opt.* **2009**, *96*, 215.
(59) Espinosa, S.; Bosch, E.; Rosés, M. *Anal. Chem.* **2000**, *72*, 5193.
(60) Calitree, B.; Donnelly, D. J.; Holt, J. J.; Gannon, M. K.; Nygren, C. L.; Sukumaran, D. K.; Autschbach, J.; Detty, M. R. *Organometallics* **2007**, *26*, 6248.
(61) Wagner, S. J.; Skripchenko, A.; Donnelly, D. J.; Ramaswamy, K.; Detty, M. R. *Biorg. Med. Chem.* **2005**, *13*, 5927.
(62) Gannon, M. K.; Detty, M. R. *J. Org. Chem.* **2007**, *72*, 2647.
(63) Schmidt, M.; Steinemann, S. G. *Fresenius J. Anal. Chem.* **1991**, *341*, 412.
(64) Pechy, P.; Rotzinger, F. P.; Nazeeruddin, M. K.; Kohle, O.; Zakeeruddin, S. M.; Humphry-Baker, R.; Gratzel, M. *J. Chem. Soc., Chem. Commun.* **1995**, 65.
(65) Wang, C.; Berg, C. J.; Hsu, C.-C.; Merrill, B. A.; Tauber, M. J. *J. Phys. Chem. B* **2012**, *116*, 10617.
(66) Chambers, R. W.; Kajiwara, T.; Kearns, D. R. *J. Phys. Chem.* **1974**, *78*, 380.
(67) Huber, R.; Spörlein, S.; Moser, J. E.; Grätzel, M.; Wachtveitl, J. *J. Phys. Chem. B* **2000**, *104*, 8995.
(68) Wang, Y.; Hang, K.; Anderson, N. A.; Lian, T. *J. Phys. Chem. B* **2003**, *107*, 9434.
(69) Rothenberger, G.; Fitzmaurice, D.; Graetzel, M. *J. Phys. Chem.* **1992**, *96*, 5983.
(70) Maity, P.; Debnath, T.; Akbar, A.; Verma, S.; Ghosh, H. N. *J. Phys. Chem. C* **2013**, *117*, 17531.
(71) Asbury, J. B.; Anderson, N. A.; Hao, E.; Ai, X.; Lian, T. *J. Phys. Chem. B* **2003**, *107*, 7376.
(72) She, C.; Guo, J.; Irle, S.; Morokuma, K.; Mohler, D. L.; Zabri, H.; Odobel, F.; Youm, K.-T.; Liu, F.; Hupp, J. T.; Lian, T. *J. Phys. Chem. A* **2007**, *111*, 6832.
(73) Kelly, C. A.; Farzad, F.; Thompson, D. W.; Stipkala, J. M.; Meyer, G. J. *Langmuir* **1999**, *15*, 7047.